Stability and oxidation of Al mirrors coated with Xe-passivated LiF thin films

Tanner Rydalch

A senior thesis submitted to the faculty of
Brigham Young University
in partial fulfillment of the requirements for the degree of

Bachelor of Science

Dr. David Allred, Advisor

Department of Physics and Astronomy

Brigham Young University

ABSTRACT

Stability and oxidation of Al mirrors coated with Xe-passivated LiF thin films

Tanner Rydalch
Department of Physics and Astronomy, BYU
Bachelor of Science

The upcoming Habitable Worlds Observatory (HWO) by NASA needs to be able to make observations as far into the Lyman ultraviolet (LUV) range of the electromagnetic spectrum as possible. Because of its high plasma frequency, aluminum (Al) offers the best reflectance in the LUV, and thus HWO's mirrors will be coated with Al. However, aluminum oxide (Al_2O_3) is opaque to the LUV, and thus a build up of Al_2O_3 sets the reflectance of an Al surface in the LUV to near 0. To prevent this, NASA's Goddard Space Flight Center (GSFC) has proposed protecting an Al-coated mirror with a thin film of lithium fluoride (LiF), passivated with XeF_2. However, LiF has not yet been shown to protect an Al surface from oxidation, and its stability has only been tested in environments similar to a standard clearn room. Thus, we took test mirrors of Al-coated silicon wafers protected by a thin film of LiF, passivated with XeF_2 (XeLiF) and stored them in various environments controlling for temperature and humidity. We characterized their aging over three months. We find that XeLiF is stable over a period of three months in cool (T = 21°C) and cold (T = 3°C) environments for humidity levels of up to 82%. Test mirrors stored in a heated environment (T = 60°C), with any relative humidity were shown to degrade. We also show that oxidation of Al surfaces is retarded according to the thickness of a XeLiF films, and that refrigerated environments (T = 3°C) further retard this oxidation.

Keywords: Habitable Worlds Observatory, lithium fluoride, thin film, mirror, mirror reflectance, relative humidity, storage

ACKNOWLEDGMENTS

First, I would like to thank my advisor, Dr. David Allred, without whom I would not have been able to accomplish this work. Next are my colleagues at BYU, Devin Lewis, Dr. Stephen Turley, and Joshua Vawdrey who have either contributed data or given me instruction. Of course, thanks goes to BYU's College of Physical and Mathematical Sciences, specifically the Department of Physics and Astronomy, who have funded me and my research.

Thanks is also due to my collaborators at NASA's Goddard Space Flight Center, who are the first to ask the question that my research tries to answer, and who made the samples which I discuss throughout this writing. The folks in question are Manuel Quijada and Luis Rodriguez.

I also thank Mario Perez for giving me a larger understanding of the goals of HWO and for giving me instruction.

Contents

Table of Contents **iv**

List of Figures **v**

List of Tables **v**

1 Introduction **1**
1.1 Proposed Mirror Film Stack 8

2 Methods **10**
2.1 Characterization Methods 10
2.1.1 Atomic Force Microscopy 10
2.1.2 Variable-angle, Spectroscopic Ellipsometry 11
2.2 Controlling Environmental Parameters Temperature and Humidity 13
2.3 Vacuum Deposition and Xe Passivation 13

3 Results **16**

4 Discussion **34**
4.1 Conclusions 36
4.2 Future Work 36

Bibliography **37**

Index **39**

List of Figures

1.1 Calculated throughput of a telescope 4

1.2 Relative humidity as a function of temperature 7

3.1 Surface roughness of samples stored at T = 3°C 17

3.2 Surface roughness of samples stored in room temperature environment 18

3.3 Surface roughness of samples stored at T = 60°C 19

3.4 AFM scan of unaged XeLiF thin film 21

3.5 AFM scan of aged control sample 22

3.6 AFM scan of aged sample stored at T = 60°C, RH = 50% 23

3.7 Reflectance measurements of aged samples 24

3.8 Film stack model 26

3.9 Oxide growth of samples stored at T = 21°C 28

3.10 Oxide growth of samples stored at T = 3°C 29

3.11 Apparent LiF thickness for samples kept at room temperature 30

3.12 Apparent LiF thickness for refrigerated samples 31

3.13 Depolarization of two aged samples 33

List of Tables

2.1 Sample designations and their storage conditions 14

Chapter 1

Introduction

The practice of astronomy primarily depends on the ability to observe objects and astrophysical phenomena through the gathering of light. Observations are made in a number filters, which isolate ranges of the electromagnetic spectrum. One such example is the V filter, which isolates primarily visible light. Telescopes are carefully constructed such that they maximize throughput in each filter they are equipped with. Since each metal's reflectance is wavelength dependent, the metal chosen to coat a telescope mirror is greatly considered.

No space-based telescopes currently exist effective at making observations deeper into the vacuum ultraviolet (VUV) than Lyα. Because of this, many stellar and galactic phenomena cannot be observed directly. One such example is the observation of giant molecular clouds (GMC). GMCs are primarily made of molecular hydrogen (H_2), helium, and trace amounts of other chemical compounds. Their presence can dampen light from stars hidden behind them. GMCs can play a role in dynamically influencing the orbits of stars in galaxies. Of primary interest to astronomers, however, GMCs can collapse to form stellar nurseries and thus star clusters, making them a key target for study. Unfortunately, the presence of a GMC must currently be inferred from the detection of carbon monoxide (CO), which constitutes at best a trace amount of the gas in a GMC. However, H_2 is known to have a spectral band in the VUV. Thus, a telescope designed to maximize throughput

in the VUV would be uniquely able to detect the presence of GMC through direct detection of H_2, their primary molecular constituent.

NASA's upcoming Habitable Worlds Observatory (HWO) has the goal of identifying and imaging 25 habitable exoplanets. Doing so requires filtering through potential host stars by characterizing them in the Lyman regime of the electromagnetic spectrum (LUV) and then looking for both biosignatures and technosignatures in the LUV. Naturally then, HWO will need to maximize its throughput in the LUV to enable this research.

Throughput for a telescope is the light gathering power of that telescope, and is proportional to the area of the pupil of said telescope. For the sake of this discussion, however, I ignore the effect that a telescope's pupil has and instead define throughput to be the ratio of the power that enters the telescope to the power that enters the detector, stated as follows:

$$T = P_0/P_D \tag{1.1}$$

where T is the throughput, P_0 is the power incident on the pupil and P_D is the power detected by the onboard instruments. The reflectance of a surface is defined similarly to be the ratio of the reflected intensity to the incident intensity like so:

$$R = I_r/I_0 \tag{1.2}$$

where R is the reflectance, I_0 is the intensity of incident light and I_r is the intensity of reflected light. If one shines a light on one mirror that reflects onto another mirror, the final light beam has its intensity calculated as the intensity of light incident on the first mirror multiplied by the reflectance of both surfaces as follows:

$$I_{final} = I_0 R_1 R_2 \tag{1.3}$$

where I_{final} is the intensity of the light that reflected off of the second mirror, I_0 is the intensity of the incident light onto the first mirror, and R_1, R_2 are the reflectances of the first and second mirror respectively.

Following this line of thinking it is easy to conclude that the throughput of a telescope can be calculated similarly, in fact the product of R_1 and R_2 are the throughput of this simple mirror array. This is generalized as follows:

$$T_k = \prod_{n=1}^{N} R_{k,n}(\theta_{k,n}) \tag{1.4}$$

Where n is an index over mirrors in a series, N is the number of mirrors in a series, k is an index over example light rays, T_k is the throughput of light ray k, and $R_{k,n}(\theta_{k,n})$ is the reflectance calculated for a given light ray k incident at angle θ on mirror n.

Since the definition of reflectance given in Eq. 1.2 gives a ratio between 0 and 1, Eq. 1.4 implies a compounding effect that leads to a dramatic loss in throughput when either the reflectance of a mirror surface is reduced or when the number of mirrors in a telescope is increased. Note in Fig. 1.1, increasingly large numbers of mirrors lead to large drops in throughput. When one assumes that the difference in reflectance due to changes in incidence angles is negligible and that each mirror is approximately identical, Eq. 1.4 simplifies to Eq. 1.5.

$$T_k = R^N \tag{1.5}$$

One can see then that the light a telescope detects is lost in an effect that compounds geometrically with the number of mirrors in a telescope. Naturally, this effect is minimized in the limit of $R = 1$ for all numbers of mirrors, making any tiny increase in reflectance precious for the aims of HWO, especially if HWO has a high number of mirrors.

Due to its high plasma frequency, the best candidate material to coat the mirrors of the next-generation telescopes is aluminum (Al). Al is highly reflective for almost all wavelengths until

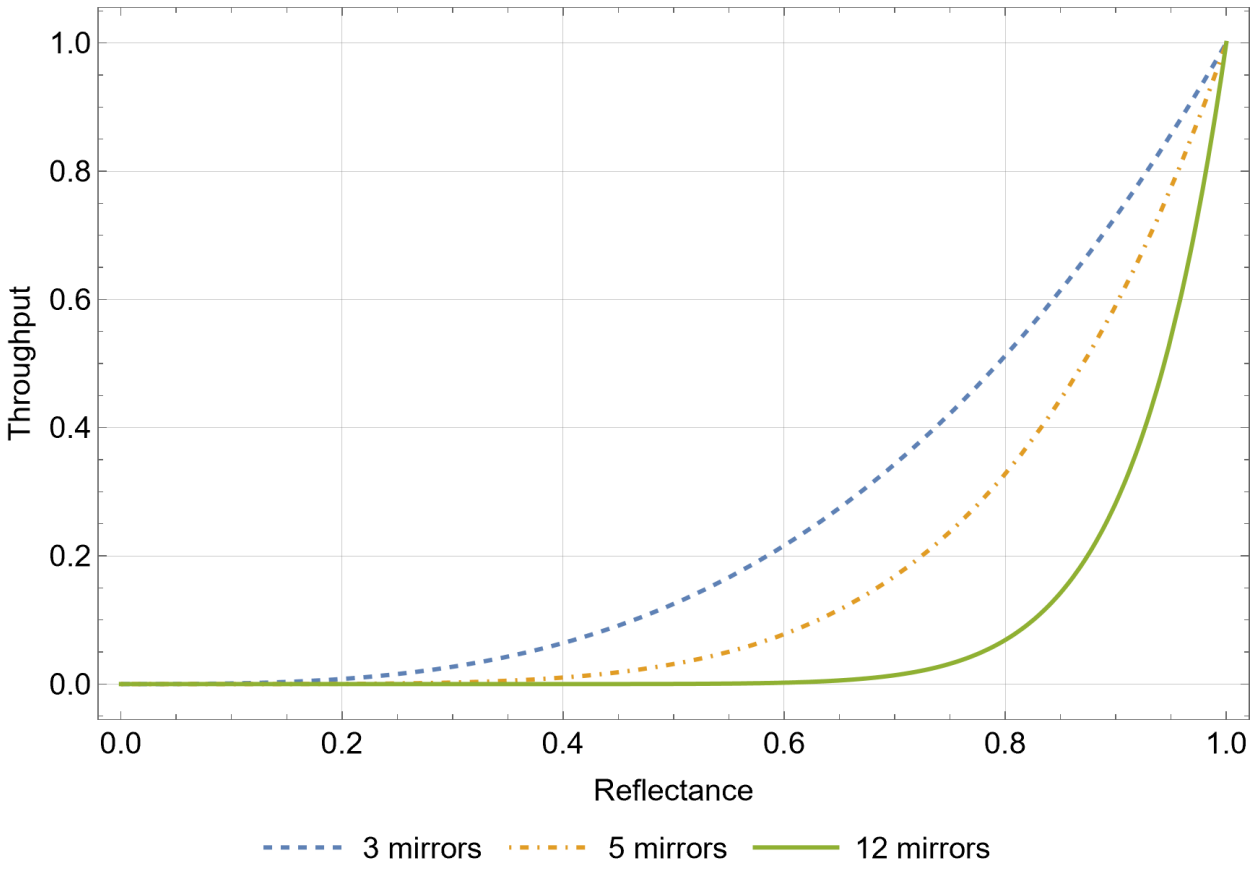

Figure 1.1 Calculated throughput of several hypothetical telescopes. The three curves above are the simulated throughput values of a telescope as a function of the reflectance of its telescope mirrors. Each curve has a different number of mirrors in its array to demonstrate the compounding effect that a loss in reflectance can have for telescopes with a large number of mirrors. For this calculation, it is assumed that variations in reflectance due to incident angles is negligible and that each mirror is made of the same material such that R for each mirror have the same value, reducing Eq. 1.4 to $T_k = R^N$. It is fairly common for advanced telescopes have a large number of mirrors in their construction, with spectrometers having a dozen or more mirrors. Thus, one can see that the compounding loss in the intensity of light creates an imperative need to choose a mirror with as high a reflectance in the targeted regime as possible.

about $\lambda \leq 100$ nm, at which point the reflectance drops to near 0. However, a thin film of aluminum oxide is opaque to the LUV regime. Aluminum oxide grows in thickness logarithmically, faster at first and then slower as time progresses, as is shown in Smith et al. [1]. Because of this, very little time is needed for a film of aluminum oxide to grow on the Al surface and destroy its LUV reflectance Since telescope mirrors tend to spend significant time in Earth's atmosphere, whether ground-based or space-based, they have plenty of time for the Al coated mirrors to oxidize. Thus, a need exists to protect the Al mirrors of the next generation space telescopes during creation and storage.

NASA's current plans to protect these mirrors are to create a thin mechanical barrier between oxygen in the atmosphere and the Al mirror. Naturally, the materials used to protect the mirror surface need to be transparent to a wide range of wavelengths, and most especially in the LUV. Among the candidate materials for this are magnesium fluoride (Mgf) and lithium fluoride (LiF).

The Hubble Space Telescope's mirrors were coated in a thin film of Mgf [2], giving Mgf protective barriers a technology readiness level (TRL) of 9, the highest possible TRL. However, Mgf does not have as high a band gap as LiF does [3], making LiF-coated mirrors more desirable for astronomers, as it will maximize HWO's throughout through a wider range of the LUV. For this reason, LiF is the first choice material to coat Al mirrors.

Unfortunately, LiF has several hygroscopic properties that have the potential to ruin thin LiF films. Firstly, LiF has a tendency to adsorb water from the air and then dissolve in it. This allows for restructuring of the film most likely through Ostwald ripening. Since the energy penalty of constructing a single large crystal is smaller than the penalty for constructing many smaller crystals, larger crystals grow at the expense of smaller crystals when some mechanism exists to transport material from smaller crystals to larger crystals. The mechanism, we believe, would be provided by any adsorbed water collected onto the film, which would dissolve the LiF, allowing Li and F ions to move through the water via diffusion, migrating from smaller crystals to larger crystals, causing

reordering of the film and an increase to surface roughness. It is known that processes such as this can cause damage to building materials [4] and transport salt throughout the structure of a porous object [5].

Relative humidity (RH) is defined to be the ratio of the partial pressure of water vapor to the saturation vapor pressure as follows:

$$RH = P_P/P_V \tag{1.6}$$

where RH is the relative humidity, P_P is the partial pressure of water vapor and P_V is the vapor pressure of water. The saturation vapor pressure can be calculated from one of several empirical fits, such as the Buck equation [6]:

$$P_V(T) = 6.1121\ \exp((18.678 - \frac{T}{234.5})(\frac{T}{257.14+T})) \tag{1.7}$$

where $P_V(T)$ is the saturation vapor pressure in hPa and T is the ambient temperature in degrees Celsius.

RH values can change either by changing the P_V or the P_P of water vapor. Figure 1.2 shows how changing the ambient temperature while holding P_P constant changes the value of RH. When the partial pressure of water vapor is less than the vapor pressure (RH < 1) any available water will evaporate, increasing the P_P, and causing RH to approach 1 asymptotically. A value of RH = 1 is defined to be saturation, and any value of RH > 1 is a supersaturated environment. In this condition, water in the air will change phase from a gas to a liquid, forming condensation when a nucleation site is available. For this reason, the dew point is defined to be the temperature that causes RH = 1, or in other words, the temperature that causes the P_V to have the same value as P_P. Examples of nucleation sites are dust grains in the air or pores in hydrophillic materials. In the latter example, condensation can occur even with an RH value less than 1, leading to adsorption. Since LiF is hydrophillic, it can adsorb water from the air at a RH of less than 1. This, combined with

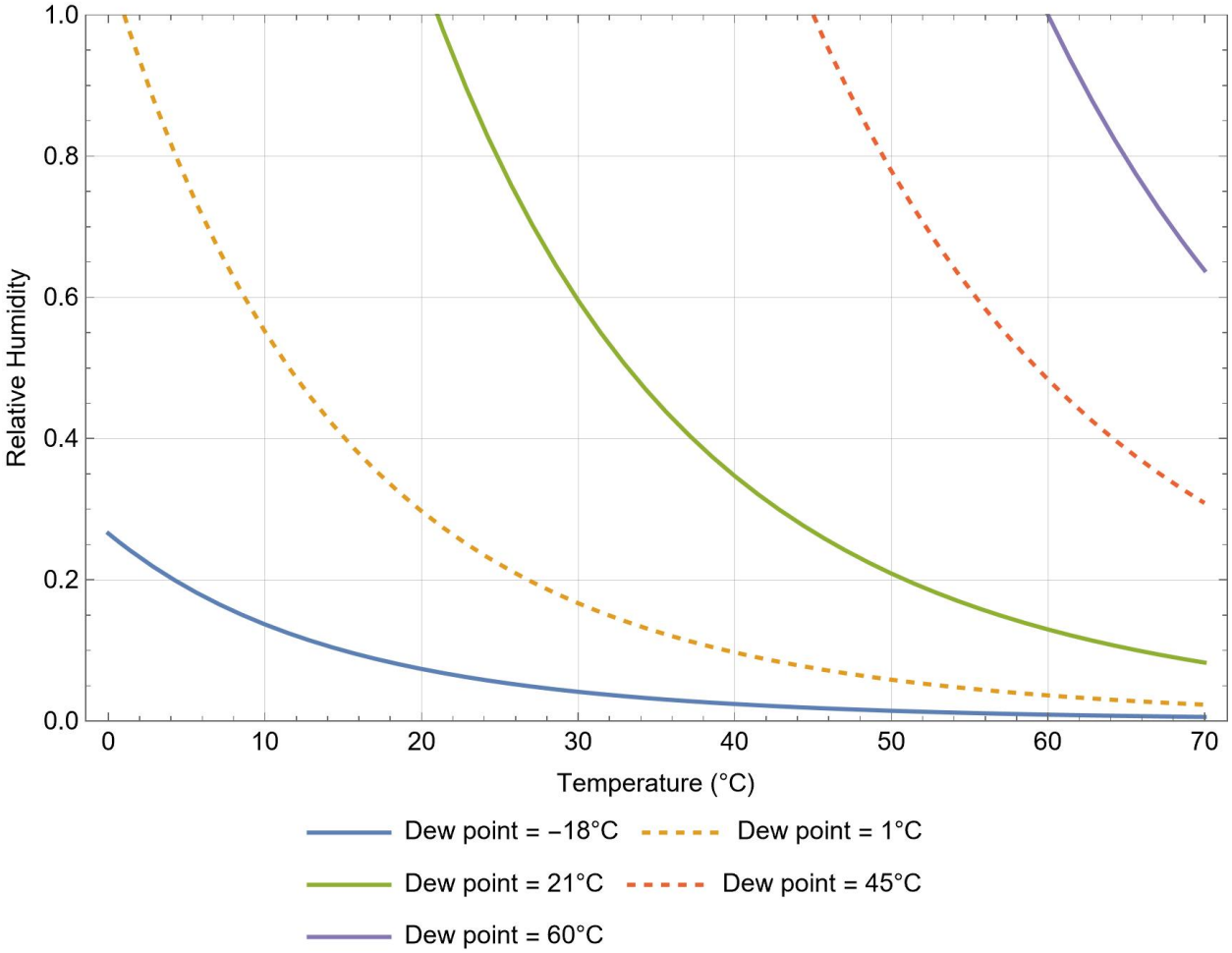

Figure 1.2 Calculated relative humidity as a function of temperature. Each line is curve of constant dew point in a temperature range going from T = 0°C to T = 70°C. Curves are calculated by combining equations 1.6 and 1.7. Evidently, as temperature increases RH decreases for constant dew points, and the inverse is also true. As temperature decreases, RH increases up to the limit of 1. At RH = 1 the environment is saturated with water vapor and the vapor in the air condenses at nucleation sites.

LiF's solubility in water creates a mechanism for transportation of Li and F ions, and allowing for Ostwald ripening to reorder the film. If this reordering causes the surface to become rougher, then pores can deepen, accumulating more water and causing a runaway effect damaging the film and exposing the substrate beneath.

Surprisingly little is known of LiF's hygroscopic properties, thus it is not known if a thin film of LiF is stable over long periods of time, and at what temperatures and humidities it is stable. If a LiF film can reorder or degrade over the duration of its storage, thinner regions may be introduced into the film–or complete exposure of the Al substrate–through Ostwald ripening, weakening the protection offered by the film. Thinner regions in the film may allow oxygen to break though to the substrate, but definitely will interfere with the carefully planned optics of the film stack. Thus, a substantial surface roughness of the LiF film is a key indicator of film failure. Meanwhile, reordering of the film such that the substrate is exposed to the environment constitutes a catastrophic failure of the film to protect its Al substrate.

Failure of any film chosen to protect the telescope mirror will cause a dramatic drop in the throughput of HWO for the effected range, which is expected to be in the LUV, effectively crippling HWO's ability to observe bio and technosignatures. Thus, my work presented in this thesis is oriented towards verifying that LiF thin films can serve as effective protective barriers for Al mirrors provided that they are not stored in an environment with an inappropriate temperature or humidity, as well as identifying which temperatures and humidities are inappropriate for LiF thin films. This will advance the TRL of LiF-coated films for use in space applications.

1.1 Proposed Mirror Film Stack

The film stack (the order and structure of films) primarily being considered by NASA consists of a glass substrate ground to the proper shape, coated by a thin (but optically thick) film of Al. The

mirror will then be passivated by exposure to xenon difluoride (XeF_2), which upon reaction with the Al film forms a thin (25-30 Å thick) film of aluminum fluoride (AlF_3). The film is then capped with a thin film of LiF, chosen to be 180 Å in thickness. During this step, Xef is allowed in the deposition chamber, which upon reacting with vaporous LiF greatly reduces the impurities introduced during a standard LiF deposition. This produces a film stack similar to that depicted in Fig. 3.8.

Each parameter has been carefully considered to maximize throughput in the VUV. For example, the index of refraction for LiF in the VUV is $n \approx 1.7$. At a wavelength of about $\lambda = 125$ nm, the wavelength of light in the LiF film is about $\lambda = 73.5$ nm, giving a quarter-wave interference, boosting the reflectance of the film stack in the effected regime.

Chapter 2

Methods

To test the stability of Xe-passivated LiF (XeLiF) thin films and their viability as protective barriers for reflective Al surfaces, Goddard Space Flight Center (GSFC) fabricated a test mirror and shipped it to BYU for study. At BYU, the test mirror was cleaved into several pieces, which were stored in various environments whose temperature and humidity were controlled.

2.1 Characterization Methods

The key indicators of film stability are taken to be the surface roughness of the XeLiF film and the presence of aluminum oxide in the film stack. The two primary characterization methods used to discern these indicators are atomic force microscopy and variable-angle spectroscopic ellipsometry, discussed as follows.

2.1.1 Atomic Force Microscopy

Atomic force microscopy (AFM) is a characterization method that gives a topographical map of a sample surface. From this map data, one can derive several different properties of the scanned region

of the sample, such as the root-mean-square (rms) surface roughness of the scanned region, which is taken as a key indicator for film stability. Three scans were taken per sample per week, with each measurement point chosen randomly from across the sample surface, and the rms roughness from these scans was averaged, with the standard deviation used to estimate variation in film roughness.

The standard scan parameters used are as follows: scan size of 2 μm by 2 μm, a scan rate of 0.5 Hz, a horizontal resolution of 1024 pixels, and a vertical resolution of 256 pixels. This vertical resolution was chosen to minimize the time that samples spent outside of storage. As can be seen in Fig. 3.6, some surface features observed are larger than the standard scan area. When appropriate, the scan size was increased to study these features. Only AFM scans with the scan size were included in Fig. 3.2, 3.1, and 3.3. The AFM used in this experiment is a Veeco™ Dimension 5000, with Aspire™ conical AFM tips, part number CT300R-25. Data from AFM were processed using Gwyddion, an open source software.

2.1.2 Variable-angle, Spectroscopic Ellipsometry

Variable-angle, spectroscopic ellipsometry (VASE) is noninvasive characterization method that uses the interactions of matter and light to probe the properties of optically thin films. A beam of light, linearly polarized at 45° across multiple photon energies from about 1.2 eV to about 6.5 eV reflects off of a sample fastened to a measurement stage via suction. As the beam reflects off of the sample, the polarization of the beam changes from linearly polarized to elliptically polarized, varying as a function of beam wavelength. This change in polarization is reflected as changes in two parameters: ψ and Δ. The equation that governs ellipsometry is as follows:

$$\frac{r_p}{r_s} = \tan(\psi)\exp(i\Delta) \tag{2.1}$$

where r_p is the Fresnel coefficient for p-polarized light and r_s is the Fresnel coefficient for s-polarized light. One can see that Δ is a phase parameter, while ψ affects the amplitude of the ratio $\frac{r_p}{r_s}$ [7].

A model is produced by stacking layers within a computation package and specifying the layer optical constants. An example relevant to this experiment is a layer with the optical constants of LiF. The software of choice is then able to fit properties that are specified by the user such as layer thicknesses or surface roughness. The user iterates on the model until satisfied with the results. It is important to note that surface roughness calculated by VASE and the rms surface roughness calculated by Gwyddion are not the same value. It is common in VASE to calculate surface roughness as an effective medium layer (EMA), which blends the optical constants of 2 or three materials at a ratio that best fits the data. CompleteEASE specifies the roughness layer to be an EMA of 50% void and 50% surface material, fitting only for thickness. The surface roughness calculated in VASE and the rms roughness are often proportional to each other by a factor of about 2.3, but only when a model is able to properly fit the data. In the case of a severely degraded sample the model developed in VASE may fail to characterize the sample, while AFM may still be used to calculate the rms roughness.

The primary function of VASE in this experiment is to monitor for aluminum oxide growth, the presence of which indicates a failure of the film to protect the Al surface and thus poor reflectance in the LUV. Since VASE cannot probe into the LUV because of atmospheric cutoff, the LUV reflectance of samples can only be inferred from this measurement technique, with confirmation coming from direct reflectance measurements.

The measurement parameters are as follows: 10 second exposure from 1.2 eV to 6.5 eV at incidence angles from normal starting at 54° to 81°, with 3° steps. The spectroscopic ellipsometer used in this experiment is a J.A. Woollam inc. M-2000, and the software package used to process the data is CompleteEASE by J.A. Woollam inc.

2.2 Controlling Environmental Parameters Temperature and Humidity

The two variables controlled in this experiment are relative humidity (RH) and temperature. Glass desiccators were modified to control for humidity by either placing a desiccant of Drierite™ ($CaSO_4$) or by placing one of several saturated salt solutions in the desiccators. Saturated salt solutions were prepared by mixing water and LiF in a small plastic container, in this case a petri dish, until well mixed and well saturated. Temperature was controlled by placing each of the prepared desiccators in one of three temperature-controlled environments, a refrigerator, ambient lab air, and an oven—nominally at 3-4°C, 20-21°C, and 60°C respectively. Sample designations, storage conditions, and the salt used to control for humidity are given in Table 2.1. Since the solubility of a salt increases with temperature, saturated salt solutions stored in the oven were prepared, brought to temperature, and then more salt added to ensure saturation. Salts were chosen using Greenspan's [8] compilation on saturated salt solutions.

2.3 Vacuum Deposition and Xe Passivation

Samples were fabricated at GSFC by thermally depositing a thin film (250-300 Å) of aluminum (Al) onto a circular wafer of silicon (Si), eight inches in diameter. After the Al deposition, samples were exposed to a sparse xenon difluoride (XeF_2) gas, passivating the Al surface and creating a thin film of aluminum trifluoride (AlF_3). The wafer then had a thin film (nominally 180 Å) of LiF deposited onto the wafer. During this, a small amount of XeF_2 gas was maintained in the deposition chamber, preventing impurities from forming in the LiF. The sample wafer was then removed from the chamber, a small sample was cleaved from the wafer for use as a witness coupon, and reflectance data were taken on the witness coupon using a MONARCH monochrometer at GSFC. The rest

Sample Designation	temperature	Relative Humidity	Control Material
a	21° C	3%	$CaSO_4$
b	21° C	33%	$MgCl_2$
c	21° C	40%	K_2CO_3
d	21° C	59%	NaBr
e	21° C	73%	$SrCl_2$
f	3° C	3%	$CaSO_4$
g	3° C	32%	$MgCl_2$
h	3° C	44%	K_2CO_3
i	3° C	60%	NaBr
j	3° C	82%	$SrCl_2$
k	60° C	3%	$CaSO_4$
l	60° C	29%	$MgCl_2$
m	60° C	50%	NaBr
n	60° C	62%	$SrCl_2$

Table 2.1 Sample test mirror designations with the temperature and humidity that the sample was stored in. The fourth column contains the material used to control for humidity. In each case, the salt was dissolved in distilled water until the water was saturated. The exception is $CaSO_4$, which was simply placed in a coarse, anhydrous form at the bottom of the desiccator.

of the sample wafer was placed in a shipping container within two minutes of the chamber being opened, whereupon the shipping chamber was nitrogen purged to displace both oxygen and water vapor, minimizing exposure to both during the early aging of the sample wafer.

The sample wafer arrived at Brigham Young University (BYU) four days later, but due to the time-sensitive nature of the sample wafer, opening the shipping container and thus exposing the sample wafer to atmospheric conditions was delayed 10 days until all basic characterization methods (AFM, VASE, and scanning electron microscopy (SEM)) could be employed in as short a time window as possible. Data were taken using VASE at several points across the sample wafer, with 12 AFM scans taken of the as-received wafer. The data taken across the surface of the as-received sample wafer were used to take statistical averages of the sample surface for use as a starting point for characterization. Because the electron beam from SEM causes degradation of sample surfaces, SEM data were not taken for the as-received wafer.

Following these procedures, we cleaved the sample wafer into 14 test mirrors, each about 1 inch by 2 inches. Some excess samples were also cleaved for use in sacrificial measurements, such as SEM, XPS, and EDX, and data were taken on these samples set aside for sacrificial measurements. The 14 primary samples were placed in one of 14 different Teflon sample holders, which were labeled and placed in one of 14 sealed environments, at three different temperatures and at 4-5 humidity levels within those temperatures.

Samples were then measured regularly for three months using AFM and VASE. Samples were removed from their storage conditions only for measurements to be taken. Data were aggregated and processed to observe trends over the course of the experiment.

Chapter 3

Results

Figures 3.1, 3.2, and 3.3 show the time evolution of the rms roughness of samples in various environments. Each data point is the average of the rms roughness of three randomly selected points across the sample surface, scanned using AFM. Notice that samples a-e (room temperature, Fig. 3.2) all appear to be somewhat stable over time, varying from week to week, but with little overall change in rms roughness, indicating relative stability over a period of three months. The same can be said of samples f-j (T = 3° C) in Fig. 3.1, except these were more stable over the experimental period than any other set of samples, for all humidity levels, even as high as RH = 82%.

All samples tested proved to have a surface roughness stable except for those stored in an oven. As seen in Fig. 3.3, all samples stored at T = 60° C became rougher over the course of the experiment, with the exception of the driest sample, sample 'k'. Sample 'm' (T = 60° C, RH = 50%) exhibits the most extreme variance over time, increasing in rms roughness, with a large variance indicative of sample non-uniformity.

Figures 3.1, 3.2, and 3.3 summarize about 300 AFM scans, and thus leave out important details, such as the shape and structure of surface features. Figure. 3.4 is an AFM scan of the sample wafer as received by GSFC, and is taken to be a representative scan of all samples before being cleaved

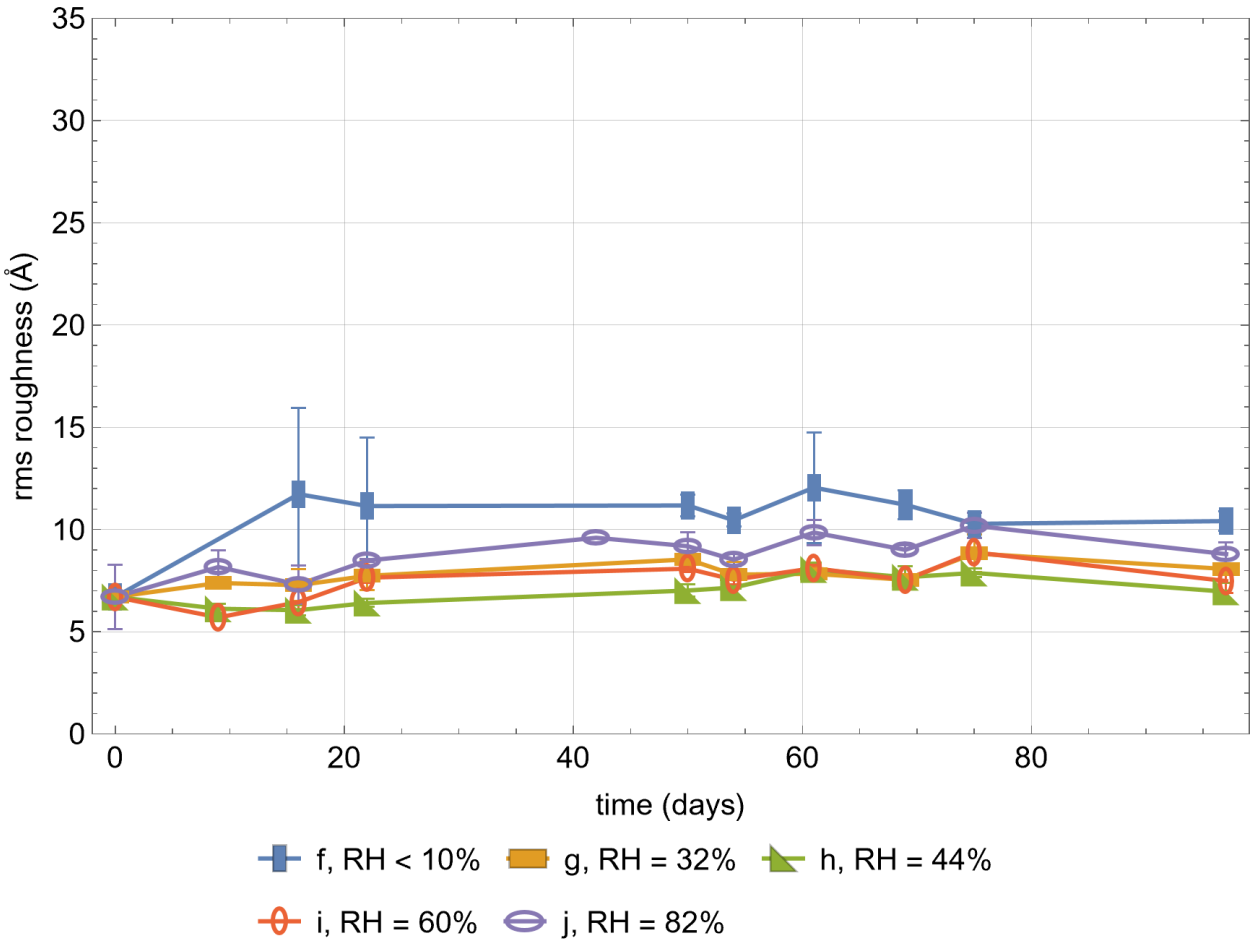

Figure 3.1 Average rms roughness over time for test mirrors stored in a refrigerator, with nominal temperature T = 3°C. Roughness values are calculated from AFM data using the open source software Gwyddion. Each data point is the statistical average of the rms roughness of three scans of randomly selected points of the given sample. Bars represent the one σ standard deviation. Note that at this temperature, rms roughness appears to be constant over time, save for the initial jump for sample 'f' (RH = 3%). This is notable, especially when compared to samples in Fig. 3.2 and Fig. 3.3. This suggests that colder temperatures cause XeLiF to be more stable over time.

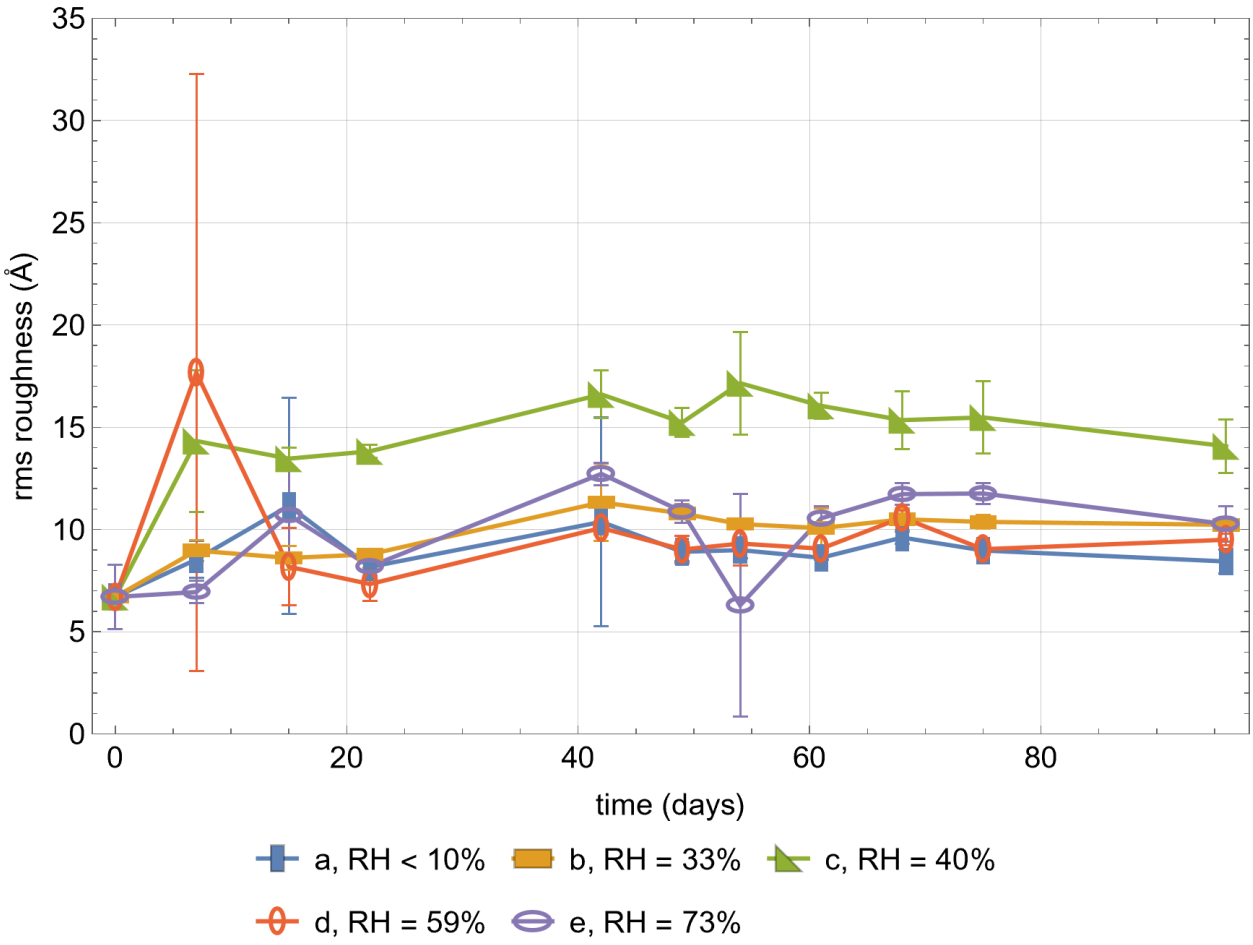

Figure 3.2 Average rms roughness over time for test mirrors stored in desiccator held at room temperature, with nominal temperature T = 21°C. Roughness values are calculated from AFM data using the open source software Gwyddion. Each data point is the statistical average of the rms roughness of three scans of randomly selected points of the given sample. Bars represent the 1 σ standard deviation. Samples appear to become slightly rougher over time, after an initial jump in rms roughness at t = 7 days, but with a seemingly stable rms roughness after that. Both these samples and those stored in a refrigerator (see Fig. 3.1) appear to be stable over the period of the experiment, suggesting that colder temperatures give XeLiF more stability.

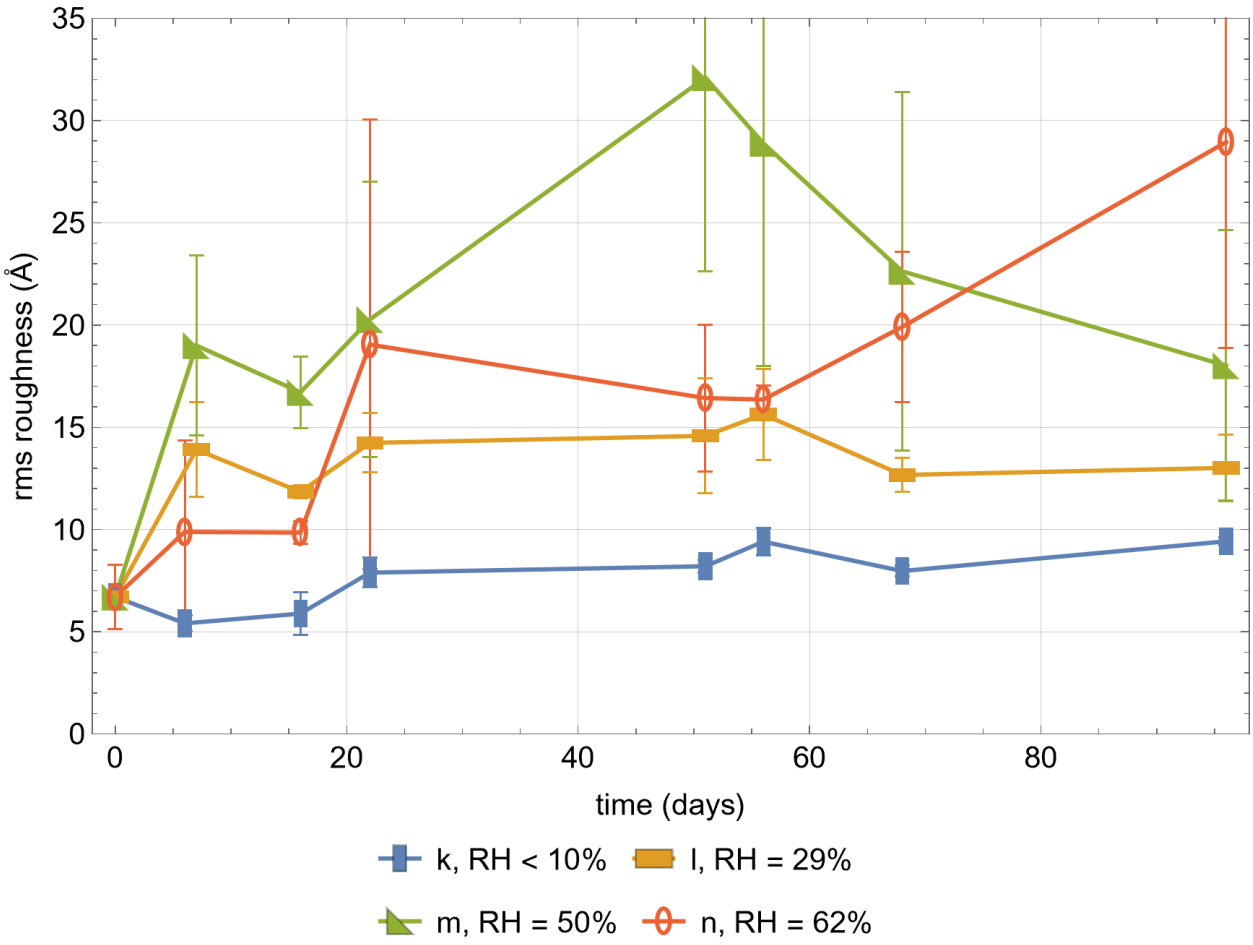

Figure 3.3 Average rms roughness over time for test mirrors stored in an oven, with nominal temperature T = 60°C. Roughness values are calculated from AFM data using the open source software Gwyddion. Each data point is the statistical average of the rms roughness of three scans of randomly selected sample points of the given sample. Bars represent the 1 σ standard deviation. All samples at this temperature became rougher during the experiment, save in the case of sample 'k' (RH = 3%). This sample seems to have been stable over the course of the experiment, with an rms roughness comparable to those found in Fig. 3.1, suggesting that high temperatures need to be coupled with humidity to be detrimental to XeLiF.

and entering storage in their various conditions (thus it has no designation). Comparing this scan to other scans from aged samples we observe some changes.

Figure 3.5 is an AFM scan of sample 'a' (T = 21°C, RH = 3%) after storage for three months, and Fig. 3.6 is an AFM scan of sample 'm' (T = 60°C, RH = 50%) aged for the same amount of time. Sample 'a' now has surface features that are rectangular in shape. Notably, these rectangular shapes were not detected in the unaged wafer before cleaving, but has been observed in all aged samples in all storage conditions. LiF has a cubic crystalline structure, so the only thing surprising about this is that surface grains were not seen to be rectangular in the as-received wafer from GSFC. Sample m, however, shows additional features that are indicative of damage done to the mirror. As seen in Fig. 3.6, large, plateau-like surface features take up much of the image. These types of features are visible across sample 'm' and often are larger than the standard scan area. All samples stored in an oven exhibit surface features such as this, with the exception of sample k, likely because very little water is present in this particular environment.

Such large features are likely to contribute to the dip in reflectance observed in Fig. 3.7. Three samples stored in the T = 60° C environment were measured with six other samples from the refrigerated and the room temperature environments, along with the witness coupon kept by GSFC. The three samples stored in the oven exhibit a drop-off in reflectance centered near λ = 140 nm, which is not visible for the other samples. We attribute this to plasmon excitation at the Al surface [9]. The presence of features observed in Fig. 3.6 allow for plasmon excitation to cause absorption in the VUV. If these dips were due to oxidation, the reflectance curve would be flatter, and likely near 0 in the range of λ = 140 nm to λ = 90 nm. Reflectance for all other samples exhibit some degree of variance not necessarily attributable to age, as the target thickness of the Al layer of the samples is 250-300 Å, making the Al layer not optically thick. Thus, one cannot easily discern if this variance is due to changes in the reflectance profiles of each individual sample over time or thickness non-uniformity introduced during sample fabrication.

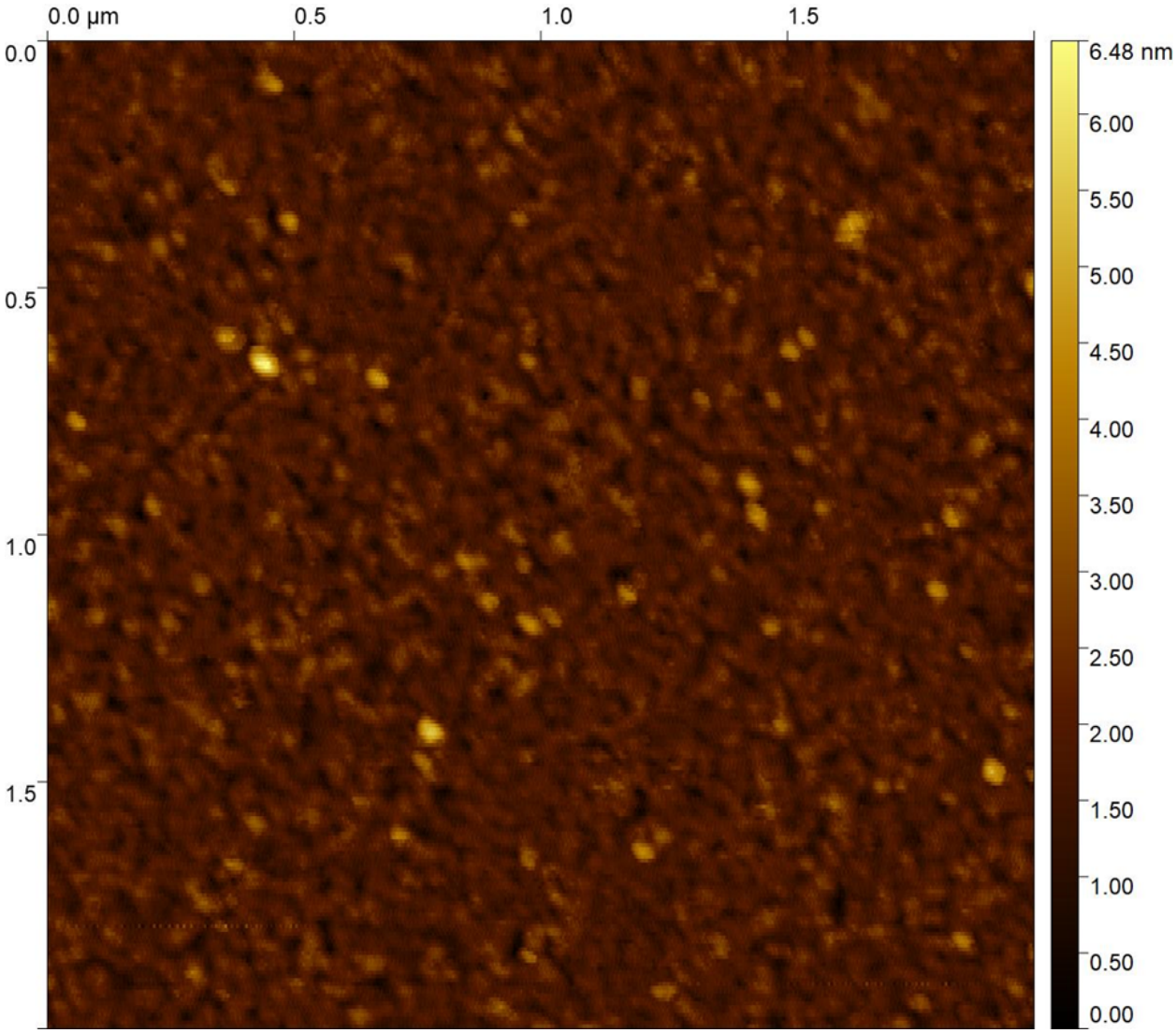

Figure 3.4 A 2 µm by 2 µm AFM scan of the XeLiF surface of the sample wafer as received from GSFC before being cleaved into the several test mirrors used in this study. This scan is representative of all samples a-n before aging, and is therefore useful for comparisons. Brighter colors mean a greater height. Note that features sticking out of the sample surface appear to be rounded. This is not the case in aged samples (see Fig. 3.5, 3.6). The rms roughness of this scan is 4.58 Å.

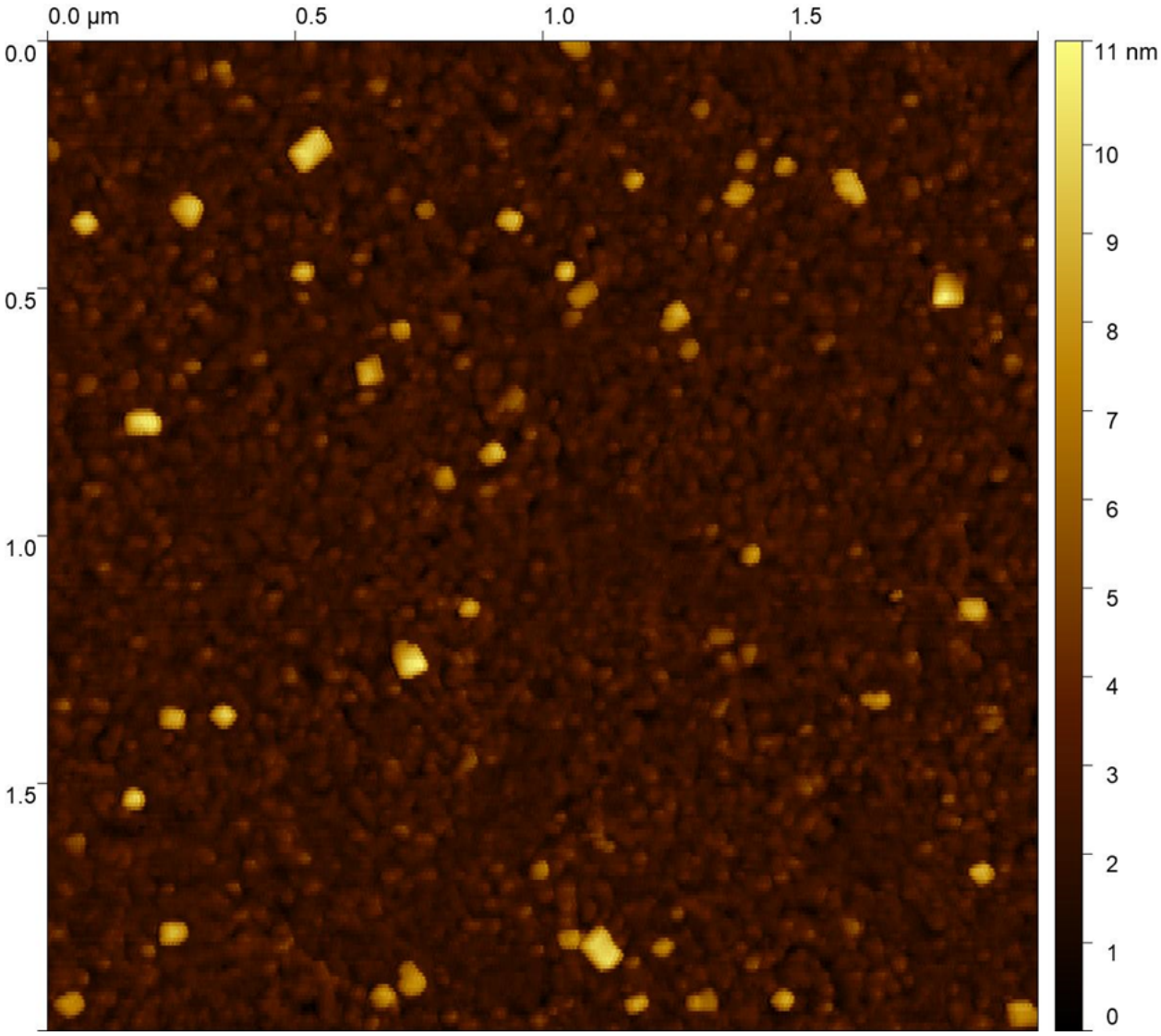

Figure 3.5 A 2 µm by 2 µm AFM scan of the XeLiF surface of sample 'a' (T = 21°C, RH = 3%), aged 2.5 months. Note that surface grains are more common than in Fig. 3.4, and that surface grains appear to be rectangular in structure. This change to rectangular shapes is observed in all aged samples. The rms roughness of this scan is 9.84 Å.

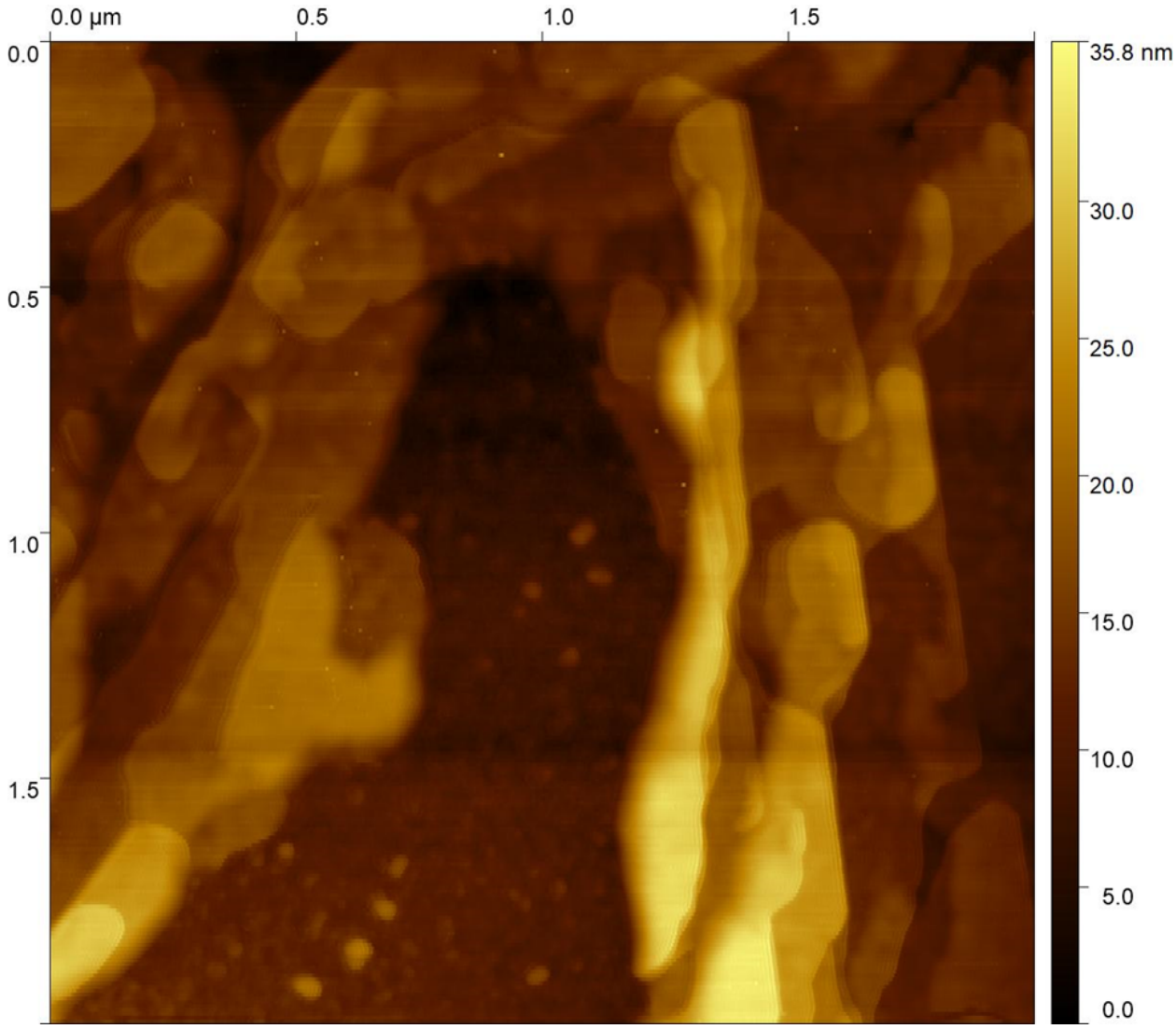

Figure 3.6 A 2 µm by 2 µm AFM scan of the XeLiF surface of sample 'm' (T = 60° C and RH = 50%), aged 2.5 months. Large, pleatau-like features such as those seen here are common on the sample, often appearing larger than the scan area. This sample is also visibly tarnished. Such large surface features likely contribute to large amounts of scattering, reducing the overall reflectance of the mirror surface. Note that the observed features appear in steps, with each plateau appearing to be relatively flat before the addition of another layer. The rms roughness of this scan is 57.4 Å, a notable difference between those shown in Fig. 3.5 and 3.4.

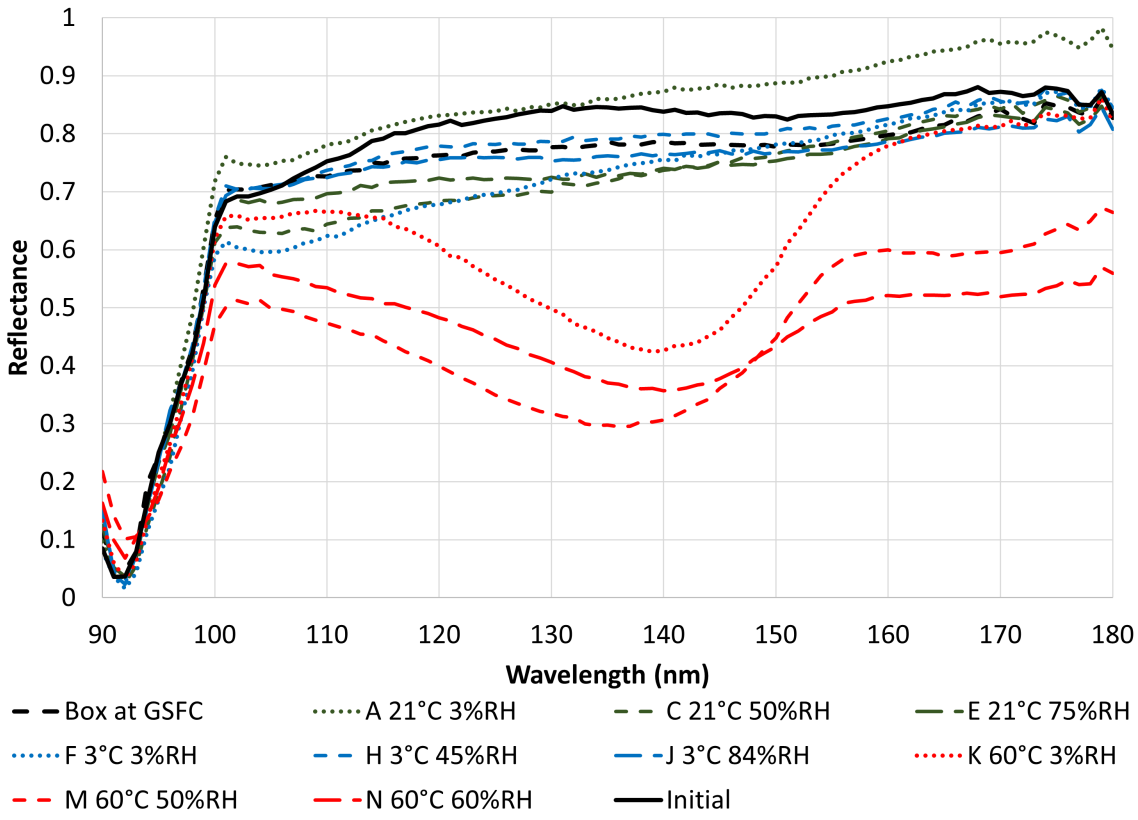

Figure 3.7 Reflectance measurements at near normal incidence for nine samples after aging for 2.5 months. The solid black line is the reflectance of a witness coupon cleaved and measured at GSFC before the rest of the wafer was shipped to BYU. The dashed black line is the same witness coupon kept by GSFC and aged in ambient air. The three samples showing a dip in reflectance centered on $\lambda = 140$ nm each were stored in an oven at T = 60°C. These dips in reflectance are likely related to the large, plateau-like features seen in Fig. 3.6.

A VASE model consisting of a substrate of Si, a thin layer of native silicon oxide, 300 Å of Al, a layer of 0 Å Al_2O_3, 27 Å of AlF_3 and 180 Å of LiF was created and thicknesses were fit for samples over time, with the exception of the AlF_3 layer. A visual representation of this is shown in Fig. 3.8. The Al_2O_3 layer was specified to be 0 Å as a starting point, and changes in oxide thickness are expected to reflect in a change in the best fit for this layer. Against expectation, the the best fit LiF layer was about 120 Å or less, depending on the sample. Some LiF films were as thin as 75 Å. GSFC's target thickness for the XeLiF film was 180 Å, and measurements such as XPS confirmed that GSFC hit this number. We do not know why VASE fits indicate a thinner LiF layer than expected. Variations from the mean are explained through sample non-uniformity introduced in the creation process. The deposition process described in 2.3 does not include planetary motion of the target wafer, which would increase uniformity across samples. This allows for variations in film thickness, but does not explain average LiF thickness being much lower than 180 Å. It is thought by GSFC that the extra fluorination provided by the XeF_2 used in sample creation changes how LiF crystals form and are packed within the film structure. It is possible that this changes LiF's optical properties enough to create a discrepancy between apparent Lif and expected LiF thickness. CompleteEASE provides correlations between fit parameters after each fit. LiF and AlF_3 have a -0.998 correlation when fitting. One Å of LiF is almost as important as one Å of AlF_3 in the fit, making it difficult to determine the thickness of each parameter since their indices of refraction are almost identical. Since communication with GSFC states that the AlF_3 thickness is 27 Å, this layer is held constant at that thickness, not allowed to fit.

As mentioned, growth of Al_2O_3 is expected to reflect in the change of the apparent thickness for the associated layer at several points in time. Figures 3.9 and 3.10 show the best fits for the oxide layer over time for samples stored in a room temperature environment and samples stored in a refrigerated environment. Samples stored in an oven are too degraded to fit a VASE model to. Figure 3.9 shows a rapid increase in the thickness of the Al_2O_3 layer for several samples, which

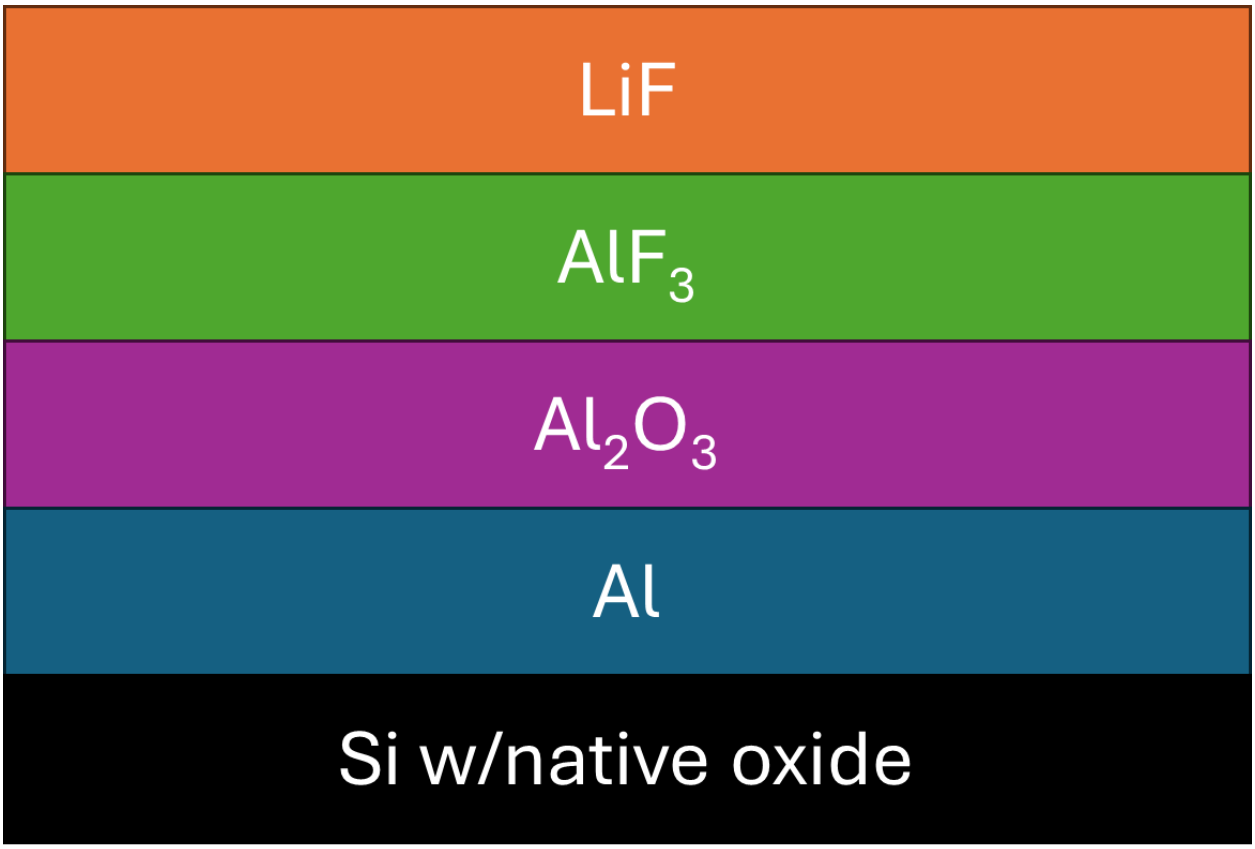

Figure 3.8 Visual representation of the VASE model used to characterize samples from GSFC. Layers are not drawn to scale. Each layer's thickness is allowed to fit, except for the Si substrate, its native oxide, and the AlF_3 layer, which is held constant at 27 Å.

then is roughly stable after that. Oxide layers are often protective films, forming a barrier that prevents further oxidation the thicker the film gets. Al_2O_3 is an example of such a film, suggesting that the increase in the film thickness follows an expected pattern.

Figure 3.10 shows a reduced amount of oxide accumulated over the same time frame for samples stored in a refrigerated environment. The exception is sample 'f'. Due to a handling error, this sample was replaced early in the experiment using an extra sample cleaved from excess wafer received from GSFC. This sample was stored in a dry desiccator stored at room temperature before being changed to a cold, dry environment. It appears that the time spent in control conditions before being moved was enough to form a thin oxide layer. All other samples stored in a cold environment showed a retarded rate of oxide growth compared to samples held at room temperature as shown in Fig. 3.9. Data from Fig. 3.1 and 3.10 in context of each other suggest that refrigerated environments are best for both XeLiF films and the reflective Al surface beneath.

Compare Fig. 3.9 with Fig. 3.11, and Fig. 3.10 with Fig. 3.12. Doing so reveals that the thickness of an oxide layer is negatively correlated with the thickness of the LiF layer in this model. This negative correlation is not as strong in Fig. 3.10 and Fig. 3.12 (which show the apparent thicknesses of films stored in a refrigerator), with the exception of sample f, which was replaced early into the experiment. This sample has both the thickest Al_2O_3 layer and the thinnest LiF layer. This negative correlation between the two films exists for all samples in a cool or cold environment. Room temperature samples show an immediate increase in oxide thickness, which then becomes roughly constant. Refrigerated environments show a slow increase in oxide thickness over time. This increase is small enough that no clear correlation between LiF thickness and oxide thickness appears.

Data from AFM has shown that heated samples have degraded on the surface, increasing in rms roughness and forming large features on the surface, as seen in Fig. 3.6. The increase in roughness of these samples has caused a large amount of depolarization at higher photon energies in

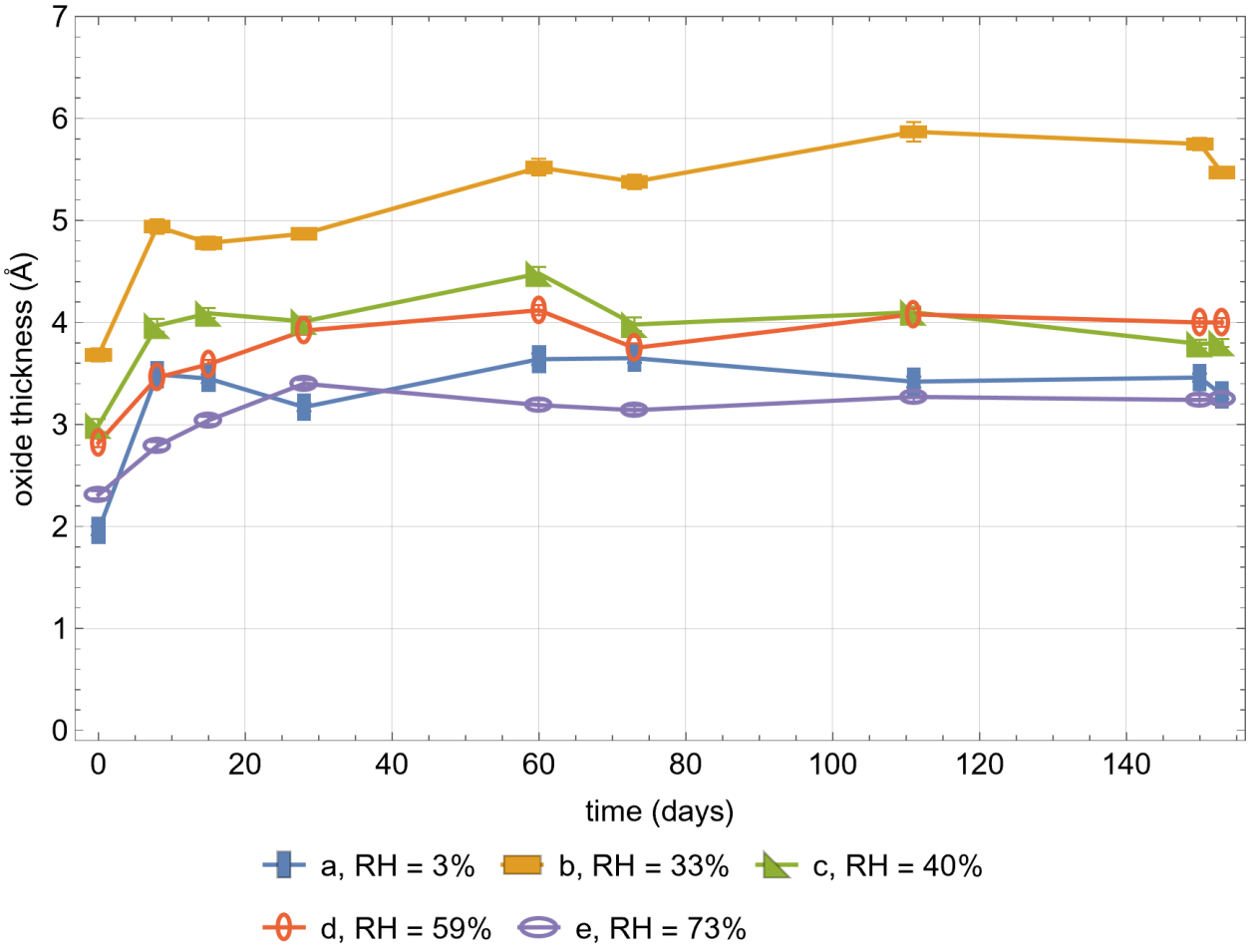

Figure 3.9 Best fits with standard error for aluminum oxide thickness obtained with CompleteEASE for samples stored in a room temperature environment at various humidity levels. Oxide thickness jumps after one week in storage, after which it appears to level out for the duration of the experiment. Figure 3.7 shows a reflectance profile in the VUV for a witness coupon cleaved from the main sample wafer, measured and kept in storage at GSFC and measured again 2.5 months later. The reflectance profile of this coupon is lower after aging for 2.5 months, but still reflective, which suggests that the oxide growth detected by VASE is present but small.

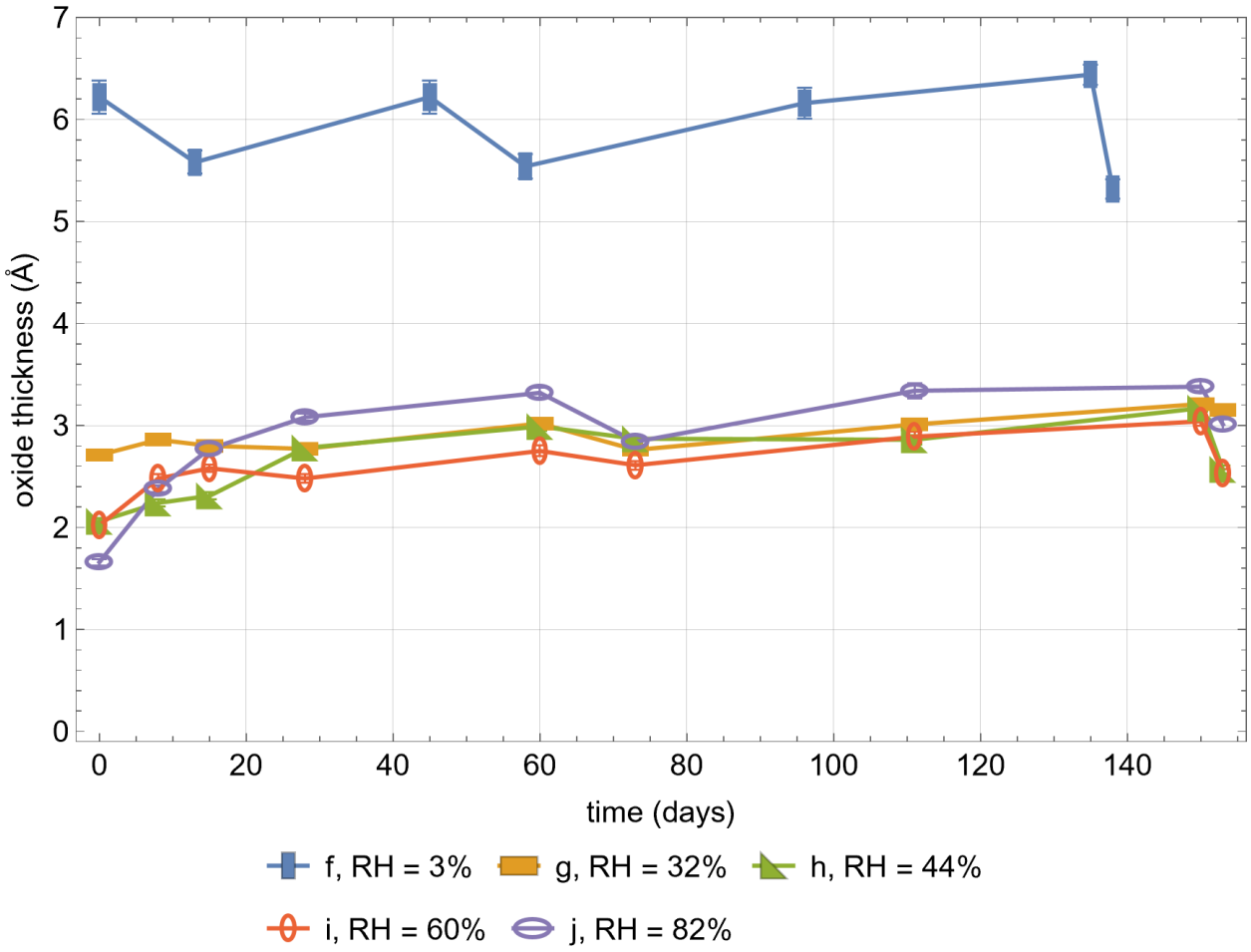

Figure 3.10 Best fits with standard error for aluminum oxide thickness obtained with CompleteEASE for samples stored in a refrigerator at T = 3°C. Oxide thickness increases rapidly in the beginning of the experiment for some samples, but then remains roughly constant further into the experiment. Note that the thickness of these oxide films is less than those in Fig. 3.9. Sample 'f' is an outlier. Because of a handling mistake, it was replaced by a spare sample cleaved from excess wafer received from GSFC that was stored in a dry desiccator at room temperature. It appears that this sample oxidized in room temperature conditions before being moved to a cold environment. This suggests that lower temperatures provide additional retardation to oxide growth.

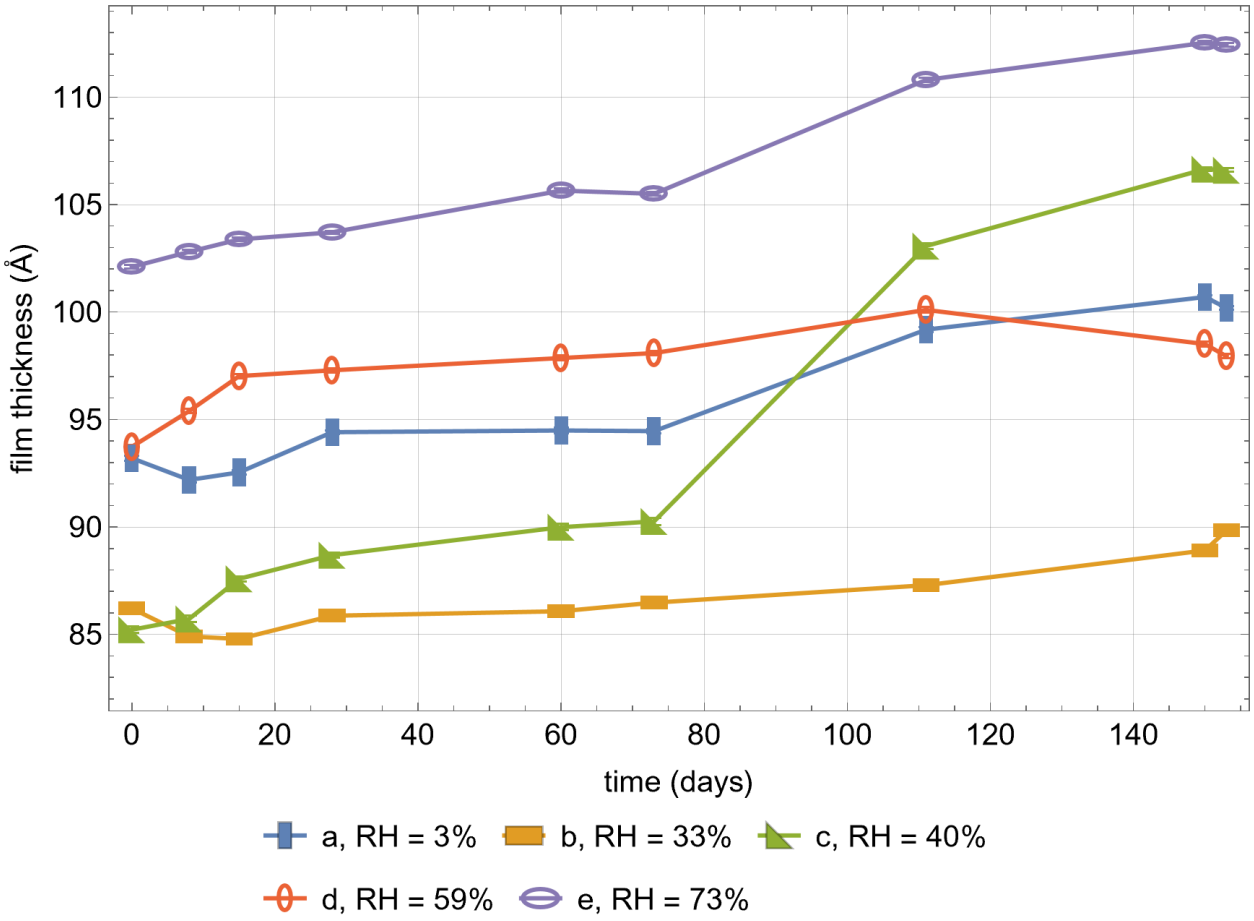

Figure 3.11 Apparent LiF thickness for samples held at room temperature, found by fitting a model to VASE data. Variations in film thickness between samples are likely due to thickness non-uniformity introduced during the fabrication of these samples. Note the general trend of an increase in film thickness. This is likely due to the incorporation of water into the film structure over time.

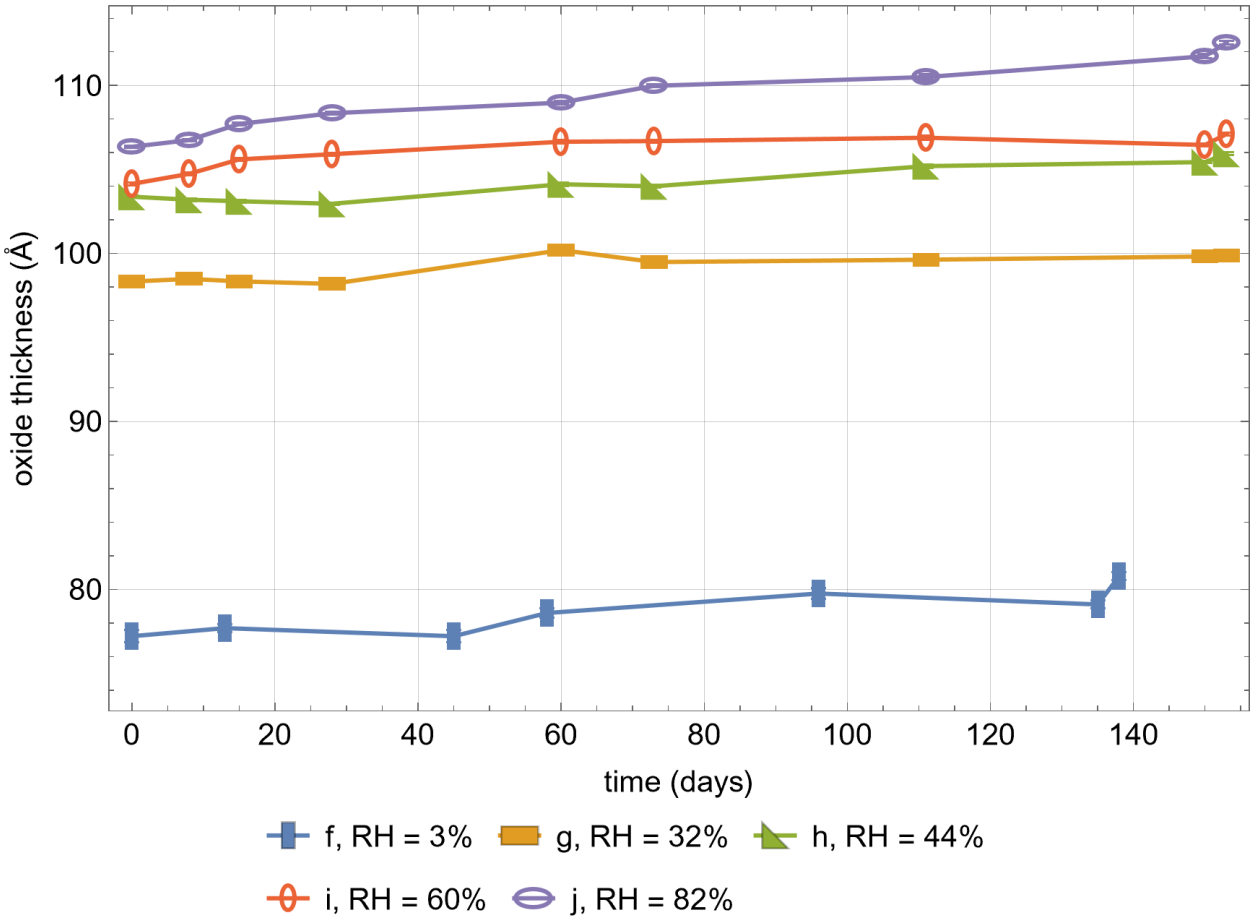

Figure 3.12 Apparent LiF thickness for samples stored in a refrigerated environment, found by fitting a model to VASE data. Variations in apparent LiF thickness are likely due to thickness non-uniformity introduced during the deposition process. Note that there is a slight increase in film thickness over time, but this film increase is less than that observed in Fig. 3.11. This increase in film thickness is likely due to the incorporation of water into the film structure.

VASE data. Depolarization in the context of VASE is the deviation from a well defined polarization, whether that polarization be linear, circular, or any degree of elliptical. The depolarization observed in heated samples increased in magnitude as the experiment progressed. This did not occur problem in other samples. Figure 3.13 compares the depolarization of sample 'a' (T = 21°C, RH = 3%) and sample 'm' (T = 60°C, RH = 50%) both aged for 3.5 months. The depolarization of a heated sample observed in Fig. 3.13 (lower) increases the complexity necessary to produce a model that accurately describes the sample. As such, no model is yet provided, and is left to future work.

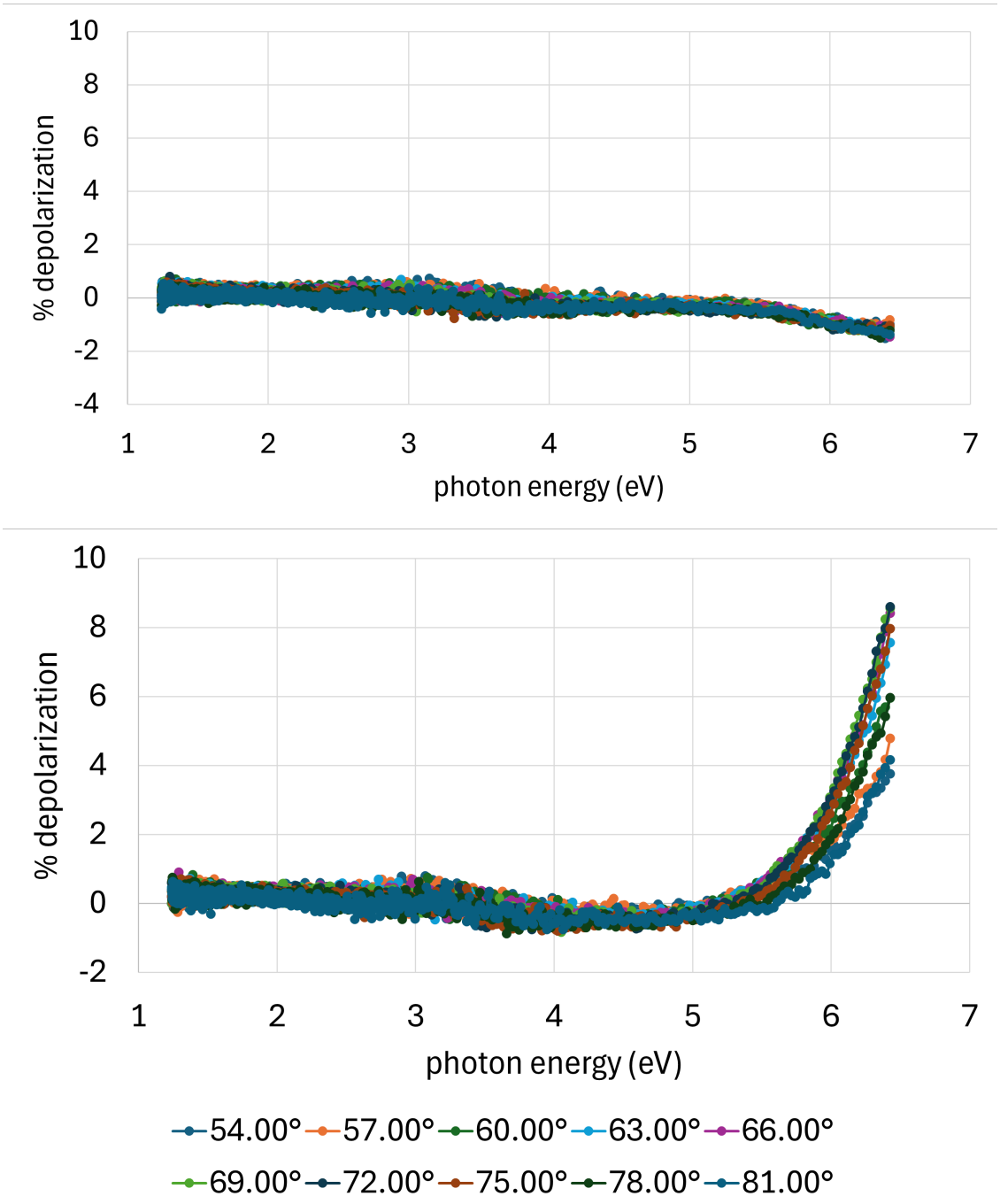

Figure 3.13 Percent depolarization according to photon energy at several angles of incidence of two samples, sample 'a' (top, T = 21°C, RH = 3%) and sample 'm' (bottom, T = 60°C, RH = 50%) measured four months after aging. Similar amounts of depolarization are observed through VASE for the other samples stored at elevated temperature. This degree of depolarization increases the complexity necessary for a VASE model to satisfy the data, and as such a VASE model cannot yet be produced for the samples stored at a temperature of T = 60°C.

Chapter 4

Discussion

The need for HWO to accomplish its goal of imaging 25 different habitable planets is dependent on having high reflectance in the Lyβ region of the electromagnetic spectrum. Several methods of protecting an Al mirror's surface from oxidation exist, such as thin films of magnesium fluoride (MgF_2), however none are transparent as far into the LUV as LiF, making LiF the most promising material to coat HWO's mirrors. By taking an Al-coated mirror, protected by a LiF thin film passivated with XeF_2 and subjecting it to various storage conditions, we are able to verify the ability of XeLiF to protect Al mirrors. Since a concern is the ability of water to reorder a LiF film over long periods of time by collection of water into pores, a key indicator of the films performance is the rms surface roughness. By measuring rms surface roughness over three months, we are able to show that this key indicator stays nearly constant over the course of the experiment, with no appreciable change in surface roughness for samples kept in an environment of T $\leq$ 21°C.

As shown in Fig. 3.2 and 3.1, samples stored in a T = 21° C and below environment display remarkable stable rms roughness values over the course of the experiment, which suggests that XeF_2 passivated LiF films are stable over time in conditions that are not hot and humid. The only samples to not display stability over time are those samples stored in an oven with T = 60°C and RH = 3%. The likely explanation for this is that the solubility of LiF increases with temperature, allowing for

more effective transport of LiF across the surface of the film. Increases in rms roughness appear to correlate negatively with reflectance, that is, when rms roughness increases, the reflectance drops. This is seen in Fig. 3.7, visible as a dip in reflectance centered near $\lambda = 140$ nm. This dip is attributable to plasmon excitation introduced by harsh storage conditions.

Since the samples tested were not optically thick, variations in Al thickness could account for the spread in reflectance observed in Fig. 3.7 for all samples except those that exhibit the dip at $\lambda = 140$ nm. Thus, one cannot naively conclude that any given deviation in reflectance from the witness sample is indicative of corrosion due to oxidation, instead that must be discerned through VASE. By fitting a model to VASE data, we discern that samples do oxidize to a small degree. However, due to variations in LiF film thickness, we see that LiF and Al_2O_3 thickness are negatively correlated, suggesting that LiF thin films do retard oxide growth, with the degree of retardation increased with LiF thickness. Oxidation is also shown to be further retarded by storage in a refrigerated environment. The small oxide film that grows could explain the drop in reflectance observed in the witness coupon kept by GSFC. All oxide films detected by VASE are shown to be on order of unity Angstroms thick, thus only a slight decrease in reflectance should be expected.

Since the XeLiF films tested have been shown to have a stable rms surface roughness over the course of the experiment, and we can see that the Al_2O_3 films have their growth retarded by LiF thin films, one can conclude that the XeLiF films produced by GSFC has sufficient capacity to protect Al mirrors over a period of three months, provided that the XeLiF film is sufficiently thick. Thus far, this experiment has lasted only a little more than three months, while HWO's mirrors are expected to spend many more months, more likely years in storage before being fully integrated and launched. Thus, while we can infer from the data available that XeLiF can protect an Al mirror for extended periods of time in the appropriate conditions, that reasonable inference cannot be verified until more experiments such as this are done for sufficiently long periods of time. Thus, all samples

used in this experiment will remain in their storage conditions and periodically measured again in several months to verify stability over time.

4.1 Conclusions

The summation of the results of this experiment and their discussion are as follows:

- Xe-passivated LiF thin films are stable in cool conditions (T $\leq$ 21°C) in all humidity levels tested (up to RH = 82% at T = 3°C) over a period of three months.
- Xe-passivated LiF thin films are unstable in a heated environment of T = 60°C for all humidity levels tested except RH = 3%. This instability is manifest as an increase in rms surface roughness and as growth of large, plateau-like features across the sample surface.
- Samples heated at T = 60°C exhibit plasmon excitation that reduces their reflectance in the VUV, centered on $\lambda = 140$ nm.
- Xe-passivated LiF thin films retard oxidation of their substrates, with thicker Xe-passivated LiF being more effective at doing so.
- Oxidation of substrates is further retarded by storage in a refrigerated (T = 3°C) environment.

4.2 Future Work

Samples will continue to be monitored at approximately three month intervals to observe changes in rms surface roughness, changes in reflectance, and growth of oxide.

Bibliography

[1] D. Smith, K. Mitchell, S. M. Hart, and D. Allred, "Retardation of the oxidation of aluminum thin films in low-oxygen and cryogenic environments,", 2023.

[2] M. Lallo, "Experience with the Hubble Space Telescope: 20 years of an archetype," Optical Engineering 51 (2012).

[3] "Chapter 3 - Thermo-Optic Coefficients," in *Handbook of Optical Constants of Solids*, E. D. Palik, ed., (Academic Press, Burlington, 1997), pp. 115–261.

[4] R. M. Espinosa-Marzal and G. W. Scherer, "Advances in understanding damage by salt crystallization," Acc. Chem. Res. **43,** 897–905 (2010).

[5] R. M. Espinosa-Marzal and G. W. Scherer, "Impact of in-pore salt crystallization on transport properties," Environmental Earth Sciences **69,** 2657–2669 (2012).

[6] A. L. Buck, "New Equations for Computing Vapor Pressure and Enhancement Factor," Journal of Applied Meteorology **20,** 1527–1532 (1981).

[7] T. Harland G. and H. James N., *Spectroscopic Ellipsometry : Practical Application to Thin Film Characterization.*, *Materials Characterization and Analysis Collection* (Momentum Press, 2016).

[8] L. Greenspan, "Humidity fixed points of binary saturated aqueous solutions," J. Res. Natl. Bur. Stand. A Phys. Chem. **81A,** 89 (1977).

[9] L. Rodriguez, Private Communication, 2024.

Index

aluminum (Al), ii, 3, 5, 8–10, 12, 13, 20, 34, 35
atomic force microscopy (AFM), 10–12, 15, 16, 20

CompleteEASE, 12

depolarization, 27, 32, 33
desiccant, 13
desiccator, 13, 14, 18

film, thin, ii, 5, 6, 8–13, 34

Goddard Space Flight Center (GSFC), ii, 10, 13, 16, 20, 21, 24, 35
Gwyddion, 12, 17–19

Habitable Worlds Observatory (HWO), 2, 3, 8, 34, 35
humidity, relative, 6, 7, 13, 16, 17, 19, 20, 23, 34, 36

lithium fluoride (LiF), ii, 5, 6, 8–10, 12, 13, 17–20, 27, 34–36

magnesium fluoride (MgF_2), 34

Ostwald ripening, 5, 8
oxide, oxidation, 25, 27, 35
oxygen, 5, 8, 15

plasmon, 20, 35, 36
polarization, 11, 32
pressure, partial, 6
pressure, vapor, 6

reflectance, reflectivity, ii, 1–5, 9, 12, 13, 20, 23, 24, 34, 35

salt, 6, 13, 14
saturation, 7, 13, 14
silicon, ii, 13, 25
solution, chemical, 13

telescope, 1–5, 8
temperature, ii, 6–8, 10, 13, 14, 17–20
throughput, 1–4, 8, 9

variable-angle, spectroscopic ellipsometry (VASE), 12, 15, 25, 26, 28, 30–33, 35